The Journal of Chemical Physics

RESEARCH ARTICLE | MARCH 18 2024

Dynamic and relativistic effects on Pt–Pt indirect spin–spin coupling in aqueous solution studied by *ab initio* molecular dynamics and two- vs four-component density functional NMR calculations

Patrick R. Batista ; Lucas C. Ducati ; Jochen Autschbach

J. Chem. Phys. 160, 114307 (2024)
https://doi.org/10.1063/5.0196853

AIP Publishing

The Journal of Chemical Physics ARTICLE pubs.aip.org/aip/jcp

Dynamic and relativistic effects on Pt–Pt indirect spin–spin coupling in aqueous solution studied by *ab initio* molecular dynamics and two- vs four-component density functional NMR calculations

Cite as: J. Chem. Phys. 160, 114307 (2024); doi: 10.1063/5.0196853
Submitted: 9 January 2024 • Accepted: 22 February 2024 •
Published Online: 18 March 2024

Patrick R. Batista,[1,a] Lucas C. Ducati,[1,b] and Jochen Autschbach[2,c]

AFFILIATIONS

[1] Department of Fundamental Chemistry, Institute of Chemistry, University of São Paulo, Av. Prof. Lineu Prestes, 748, 05508-000 São Paulo, SP, Brazil
[2] Department of Chemistry, University at Buffalo, State University of New York, Buffalo, New York 14260-3000, USA

[a] Email: patrick@iq.usp.br
[b] Email: ducati@iq.usp.br
[c] Email: jochena@buffalo.edu

ABSTRACT

Treating ^{195}Pt nuclear magnetic resonance parameters in solution remains a considerable challenge from a quantum chemistry point of view, requiring a high level of theory that simultaneously takes into account the relativistic effects, the dynamic treatment of the solvent–solute system, and the dynamic electron correlation. A combination of Car-Parrinello molecular dynamics (CPMD) and relativistic calculations based on two-component zeroth order regular approximation spin–orbit Kohn–Sham (2c-ZKS) and four-component Dirac–Kohn–Sham (4c-DKS) Hamiltonians is performed to address the solvent effect (water) on the conformational changes and $^1J_{PtPt}$ coupling. A series of bridged Pt^{III} dinuclear complexes $[L^1–Pt_2(NH_3)_4(Am)_2–L^2]^{n+}$ (Am = α–pyrrolidonate and pivalamidate; L = H_2O, Cl^-, and Br^-) are studied. The computed Pt–Pt coupling is strongly dependent on the conformational dynamics of the complexes, which, in turn, is correlated with the trans influence among axial ligands and with the angle N–C–O from the bridging ligands. The *J*-coupling is decomposed in terms of *dynamic* contributions. The decomposition reveals that the vibrational and explicit solvation contributions reduce $^1J_{PtPt}$ of diaquo complexes ($L^1 = L^2 = H_2O$) in comparison to the static gas-phase magnitude, whereas the implicit solvation and bulk contributions correspond to an increase in $^1J_{PtPt}$ in dihalo ($L^1 = L^2 = X^-$) and aquahalo ($L^1 = H_2O$; $L^2 = X^-$) complexes. Relativistic treatment combined with CPMD shows that the 2c-ZKS Hamiltonian performs as well as 4c-DKS for the $^1J_{PtPt}$ coupling.

I. INTRODUCTION

Nuclear magnetic resonance (NMR) parameters of platinum (Pt) are highly versatile experimental probes for structure and dynamics as well as for chemical bonding in Pt-containing species.[1,2] The only magnetic isotope, ^{195}Pt, has spin 1/2 and a receptivity almost 20 times larger than that of ^{13}C, rendering ^{195}Pt as one of the best explored isotopes in NMR among transition metals. The known chemical shift range of ^{195}Pt is wide, ranging from ca. −6000 to +12 000 ppm. The shift depends on the Pt oxidation state, the donor or acceptor characteristics of the coordinating ligand, the covalency of the metal–ligand interaction, and the characteristics of excited states that couple magnetically with the ground state when the systems respond to the external and internal magnetic fields that are probed in NMR experiments. Spin–spin coupling constants (*J*-coupling) involving ^{195}Pt, which are useful for determining the extent of interaction of the metal center with coordinated ligands, also vary considerably, from ~1 to 10 kHz.[3]

From a theoretical point of view, predicting ^{195}Pt NMR data poses serious challenges because the calculated parameters require a high computational level by taking into account relativistic effects and the electron correlation, among other factors.[4–11] As shown in some of the cited works, Pt NMR shifts are known to depend very sensitively on structural parameters, such as Pt–ligand distances, and when open coordination sites are present (for example, as is the case with planar complexes), the Pt center may interact directly with solvent molecules or neighboring sites in a solid. Therefore, for solvated Pt complexes, reliable calculations of Pt NMR parameters require a high-level dynamic description of solvation. The crucial importance of a dynamic treatment of solvent effects when attempting accurate predictions of Pt NMR parameters was demonstrated specifically by Autschbach and co-workers for Pt^{IV} and Pt^{II}[7,8] complexes and Pt–Tl bonded[12] systems, it was emphasized by Davis *et al.*[10] for the isotopologues and isotopomers of Pt^{IV} aqua/chlorido complexes, and, more recently, highlighted again by Castro *et al.*[13] who studied Pt–P bonded complexes.

Computational strategies have been investigated for the study of heavy-metal-containing molecules in solution and their NMR parameters.[14] A simple and commonly used model is the implicit solvation method, which only accounts for the electrostatic effects of the solvent environment on the NMR parameters through a dielectric continuum. Explicit solvation, for example, when incorporated into *ab initio* molecular dynamics (AIMD), is also widely used when the description of solute–solvent interactions at the quantum mechanics (QM) level is crucial. Furthermore, AIMD incorporates the semiclassical vibrational contributions, resulting from the classical thermal motion of the nuclei, which can influence the chemical shift of Pt and its *J*-coupling with ligand nuclei.[7–9] The combination of AIMD with Kohn–Sham (KS) density functional theory (DFT) NMR calculations for light and heavy nuclei has been successfully applied to NMR parameter investigations in solution more generally.[13,15–20]

As mentioned already, calculated Pt NMR chemical shifts and *J*-couplings are sensitive to relativistic effects. This is expected, given the high nuclear charge of Pt ($Z = 78$) and given that molecular properties arising from the hyperfine magnetic interaction between electrons and nuclei heavily weigh the relativistic effects of the valence orbitals in the outer and deep cores.[4] Relativistic calculations of NMR parameters, in particular, involve approximations in the treatment of the system's ground state as well as its response to the internal and external magnetic fields,[21] even when such calculations are labeled fully relativistic. As far as the one electron part of the Hamiltonian is concerned, the 4-component (4c) Dirac Hamiltonian, as well as "exact" 2-component (2c, X2C and variants thereof) and approximate 2c (quasi-relativistic) Hamiltonians are available for NMR calculations.[21,22] Among the latter, the zeroth-order regular approximation (ZORA) Hamiltonian[23] is in widespread use for NMR applications,[24–31] often in combination with DFT. It has been demonstrated repeatedly that heavy-element NMR chemical shift and *J*-coupling calculations can be as accurate with ZORA as they are with fully relativistic methods,[19,24,25,32–35] especially when considering the impact of the many other approximations that are necessary in molecular electronic structure and response calculations. (However, note that ZORA is not accurate for describing the relativistic effects on the absolute shielding of heavy isotopes.[24,25])

Recently, a combination of Car–Parrinello (CP) AIMD and ZORA relativistic NMR calculations was shown to produce aqueous solution ^{195}Pt chemical shifts and Pt–Pt one-bond *J*-coupling of α–pyridonate-bridged dinuclear platinum complexes in reasonable agreement with the available experimental data and more accurately than calculations utilizing static optimized geometries.[36] An analysis of the isotropic NMR results in terms of localized and canonical orbitals[37] showed that $^1J_{PtPt}$ is driven by solvent-induced changes in the *s*-character of the natural atomic orbitals of the Pt atoms, which affects the (usually dominant) Fermi contact mechanism of *J*-coupling and its relativistic analog. Interestingly, although the experimental trends were reproduced correctly, the inclusion of the spin–orbit (SO) interaction in the relativistic calculations significantly overestimated *J*-coupling values, which were larger by 2.8 kHz on average compared to scalar relativistic (SR) calculations. However, SO effects are part of a full description of the relativistic effects in a system, and therefore, there is no good reason why they should be discarded. This raises the question whether the approximations inherent in ZORA break down when dealing with the combination of relativistic effects from two Pt centers in $^1J_{PtPt}$.

Pt–Pt bonded complexes represent the rare Pt +3 oxidation state. The formal metal–metal bond is often stabilized by bridging the ligands coordinated to the platinum atoms either by two nitrogen and two oxygen atoms, namely, "Head-to-Head" (HH), or by two different ligand atoms, namely, "Head-to-Tail" (HT). In the HH configuration, the Pt centers are not equivalent (herein referred to as $Pt[N_2O_2]$ and $Pt[N_4]$), while in HT, the platinum atoms are equivalent (referred to as $Pt[N_3O]$).[38,39] Many interesting properties and potential applications have been attributed to these types of compounds.[40–50] However, as explained already, the prediction of NMR parameters for ^{195}Pt, in general, and for Pt^{III} complexes, in particular, still poses challenges for quantum chemistry.

The aim of the present study was to extend the insights, obtained recently in Ref. 36 for α–pyridonate-bridged dinuclear platinum complexes, into the solution state of the derivatives of pivalamidate- and α–pyrrolidonate-bridged dinuclear complexes shown in Fig. 1. Therefore, we concentrate our efforts mainly on the relativistic treatment and the investigation of contributions from the *dynamic* approach to the calculated $^1J_{PtPt}$ coupling. To this end, a comparison was made between the DFT calculations based on the Dirac–Kohn–Sham (4c-DKS) vs the ZORA SO Kohn–Sham (2c-ZKS) Hamiltonian, as well as the decomposition of the *J*-coupling into solvent and thermal contributions. These aspects have not been addressed in previous studies on Pt^{III} dinuclear platinum complexes. As will be shown, ZORA performs accurately for these systems, and therefore, the deviations between the calculated and experimental NMR data must arise from a combination of other approximations, highlighting the need for improved theoretical methods to treat NMR parameters of platinum and potentially other heavy transition metals.

II. COMPUTATIONAL DETAILS

A. AIMD simulations

AIMD simulations of the Car–Parrinello type were performed using Quantum ESPRESSO (QE) version 6.0.[51] The geometries of the complexes 1–10 (see Fig. 1 for the numbering) were initially optimized using the QE PW module, applying the Martyna–Tuckerman

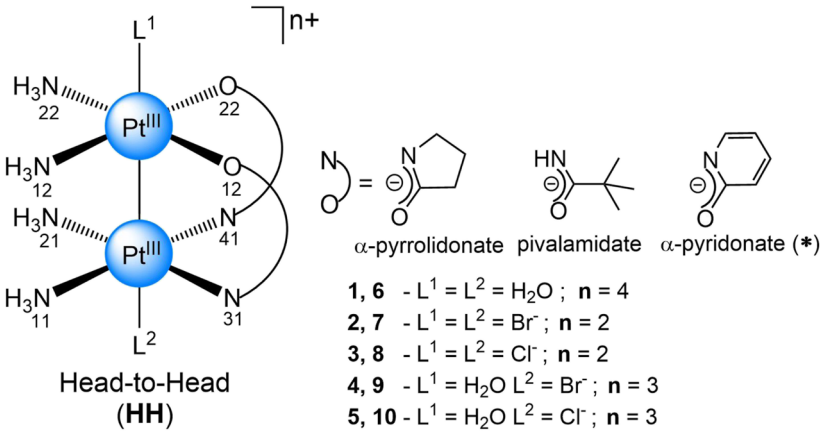

FIG. 1. Schematic representation of head-to-head (HH) Pt–Pt α–pyrrolidonate-bridged (**1–5**) and pivalamidate-bridged (**6–10**) complexes studied in this work. * α-pyridonate bridged complexes were investigated in Ref. 36.

correction, which assumes the system to be isolated (a molecule or a cluster in a 3D super cell), to yield accurate and numerically efficient descriptions of long-range interactions.[52] The simulation cells were then created using the PACKMOL[53,54] software. Each cell consisted of a single optimized complex in the center surrounded by solvent molecules. To reproduce the chemical environment of the NMR measurements,[39] perchlorate anions (ClO_4^-) were substituted for water, as needed, maintaining the neutrality of the cell and a total of 65 solvent molecules (the solute complex, water molecules, and a few perchlorate anions). Hydrogen atoms were replaced with deuterium to aid in the adiabatic separation of electronic and nuclear degrees of freedom.[55] The dimensions of the cells, L, were chosen to reproduce the heavy water density of 1.11 g cm^{-3}. The box sizes are presented in Table I.

Structure optimizations and AIMD simulations were performed with the Perdew–Burke–Ernzerhof (PBE) exchange–correlation functional.[56,57] Ultrasoft pseudopotentials from psilibrary 1.0.0[58] were used to represent each atom by its effective core and the associated valence pseudo-orbitals.[59] The trajectories were obtained with a kinetic energy cutoff of 100 rydberg, a fictitious electron mass of 450 atomic units (a.u.), and a time step of 5.0 a.u. (0.12 fs) to integrate the Car–Parrinello equation of motion.[60–62] Grimme's dispersion correction (D2)[63] was included for all atoms. After an initial wave function optimization (using the QE CP module), two simulation steps were performed, i.e., equilibration and production. Equilibration was carried out in the canonical ensemble (NVT) using a chained Nosé–Hoover thermostat[64] at a temperature of 350 K to attenuate the overstructuring produced by the PBE functional when applied to the dynamic structure of water.[55,65–67] The systems were allowed to equilibrate for ~3 ps. Subsequently, the production trajectory was simulated in the microcanonical ensemble (NVE) for 30 ps. The first 1 ps in the NVE ensemble was considered part of the equilibration. The reliability of the AIMD simulations was probed by calculating radial distribution functions (RDFs) and selecting mean distances and angles for the solute. These analyses were carried out using 24 100 AIMD configurations each from the production runs with a maximum radius (r_{max}) of 7 Å and a discrete radial grid of 0.03 Å, provided by Visual Molecular Dynamics (VMD)[68,69] version 1.9.3.

TABLE I. Simulation box compositions and sizes for the systems studied herein.[a]

System	Solute	H_2O	ClO_4^-	L/Å
1/6	1	60	4	15.27/15.35
2/7	1	62	2	15.18/15.25
3/8	1	62	2	14.96/15.04
4/9	1	61	3	15.22/15.30
5/10	1	61	3	15.12/15.20

[a]System numbering refers to the complex numbers shown in Fig. 1.

B. NMR parameter calculations

The $^1J_{PtPt}$ calculations were performed mainly with the CPL module[70–72] of the Amsterdam density functional (ADF) program version 2018.[73] The ZORA Hamiltonian was used in its SR ("1-component") version or in its proper 2c form, the latter including both the SR and SO effects, along with the hybrid functional PBE0 (containing 25% of exact exchange).[74] A Slater-type orbital (STO) basis developed for J-coupling calculations (jcpl)[57] was used for Pt atoms, while other atoms were described by an all-electron STO basis set of polarized valence triple-ζ (TZP) quality. The atomic nuclei were described as spherical Gaussian charge and magnetization distributions.[75] The conductor-like screening model (COSMO)[76] was applied to represent the bulk solvent effects in addition to, or on top of, explicit microsolvation.

The dependence of the magnetic properties as a function of the number of explicit solvent molecules was analyzed by arithmetic averaging of the J-coupling over sufficiently large solute–solvent clusters following the approach described in our previous work.[36] Additional details are provided in Sec. S2 of the supplementary material. The final statistics for $^1J_{PtPt}$ were accumulated from 256 AIMD production run configurations per complex, evenly spaced along the trajectory (every 0.11 ps), computed at the 2c-ZKS/PBE0

level. The results obtained using the AIMD configurations (termed the *dynamic* model) were then compared with those calculated using single optimized geometry (termed as the *static* model) for an isolated complex and the complex calculated using only the continuum model to represent the solvent.

Additional 4c-DKS calculations of $^1J_{PtPt}$ for complexes **1** and **6** were performed to assess the 2c-ZKS calculations. The PBE0 functional was used for consistency, along with the Gaussian-type orbital (GTO) basis set Dyall VTZ[77,78] for Pt atoms, which was shown to be efficient for NMR parameters.[79] For the other atoms, the IGLO-II[80] basis set designed for magnetic properties was applied. Because of the computational effort associated with these calculations, 64 AIMD configurations among the total of 256 that were sampled were used in the 4c set of calculations, either without any type of solvation ($AIMD^{bare}$) or explicitly solvated with the ten nearest-neighbor molecules (solvent or counter ion) in solution ($AIMD^{10NN}$), as explained in Sec. S2. Because the effects of relativity mainly affect the complexes, to reduce computational resources, the $AIMD^{10NN}$ model in the 4c-DKS calculations was adjusted with bulk solvent contributions from the corresponding 2c-ZKS data. The 4c-DKS calculations were performed using the Respect program,[81] designed to perform relativistic DFT calculations at the fully relativistic four-component level [Dirac–Coulomb Hamiltonian,[82] represented in a restricted kinetically balanced (RKB) spinor basis].

C. Conceptual separation of contributions to the solvent effect

The total solvent effect on a given ^{195}Pt NMR parameter is in principle, although not necessarily in practice, an observable and is given by the difference between the solution phase vs gas phase measurement or calculation. The solvent effect may be conceptualized by separating it into a direct and an indirect contribution. (As it is usually the case, such a partitioning is somewhat arbitrary because only the sum of all contributions is well-defined, but justified if it gives insight.) The direct effect arises from the perturbation of the solute electronic structure by the presence of the solvent. The reference point is the electronic structure of the solute in the gas phase at a given molecular geometry. For the purpose of the present work, we use the geometry of the solvated complex to evaluate the direct NMR effect. The indirect effect arises from the changes in the solute geometry in the solvent with respect to the equilibrium structure in vacuum. This change in geometry also causes changes in the electronic structure of the solute[83] and, therefore, changes in the NMR parameters. The indirect solvent effect is quantified here as the change in a given NMR parameter in gas-phase calculations when the geometry of a complex is changed from the gas-phase equilibrium geometry to the solution-phase geometry. The latter can be an individual configuration or an averaged geometry extracted from a molecular dynamics (MD) simulation of the solvated system, for example, or a complex geometry optimized in conjunction with some kind of solvent model. It is worth mentioning that the consideration of the indirect solvent effect actually involves a combination of vibrational averaging and solvation effects. While simulations in the gas phase can provide additional insights into the vibrational contribution, this study focuses on the liquid phase. We conducted a decomposition of each effect based on the $^1J_{PtPt}$ calculations in Sec. III C.

III. RESULTS AND DISCUSSION

The quality of the simulated solvent structure was gauged based on the $g(r)$[O–O] RDFs, by assuming that the structure of liquid water will be largely preserved between the complexes at not too high concentrations. Indeed, a reasonably accurate simulation of the intermolecular structure of liquid water was obtained when compared to the simulated and experimental RDFs of pure water (see Sec. S1 in the supplementary material).

The platinum–oxygen RDFs, $g(r)$[Pt–O], are shown in Fig. 2. These RDFs describe the (ligand and solvent) structure around the platinum atoms. The first set of peaks, from 2.0 to 2.7 Å shown in Figs. 2(a) and 2(c), represents the axial oxygen of the aqua ligand for the diaquo and aquahalo complexes directly coordinated with the Pt[N_4] atoms. The Pt–OH_2 interaction appears to be rather strong overall, resulting in relatively small variations of the Pt–O distances during the simulations. Correspondingly, these RDF peaks are sharp, although less so for the aquahalo complexes as compared to the diaquo complexes, presumably indicating a somewhat weaker Pt–OH_2 interaction in the former. The RDF peaks just above 3.0 Å, as shown in Figs. 2(a) and 2(c), correspond to the equatorial oxygen atoms bound to the Pt[N_2O_2] atoms; the distances are those with respect to the Pt[N_4] centers. Differences in the results for the different complexes regarding this peak are negligible. The third and fourth sets of peaks, around 4.2 and 6.2 Å, respectively, represent oxygen atoms from solvent molecules contained in the first and second solvation shells. Figures 2(b) and 2(d) show the first set of peaks around 2 Å, which represents both the axial and equatorial oxygen from the Pt[N_2O_2] moiety for all complexes. Correspondingly, these RDF peaks are considerably higher than the first RDF peaks shown in Figs. 2(a) and 2(c), while the peaks just above 3 Å are not present. The second and third sets of peaks, between 3.6 and 7.0 Å, depict oxygen atoms of the solvent molecules of the first and second solvation shells, respectively.

The RDF integrals, $N(r)$[Pt[N_4]–O] and $N(r)$[Pt[N_2O_2]–O], represent the average number of oxygen atoms found up to a distance r from the platinum center, including the oxygen atoms explicitly coordinated on platinum sites. Since we know the latter, the $N(r)$ data reveal the number of water molecules surrounding a given complex. For the diaquo and aquahalo complexes, integration of the RDFs gives 10 and 30 solvent molecules for the first and second solvation shells, respectively.

For the dihalo complexes, ~7 and 20 solvent molecules, respectively, were found. Therefore, a total of 64 solvent molecules (including counter ions in the solvent count) within the simulation box are suitable to describe the complexes in solution. Furthermore, a visual inspection revealed that the solvation occurs much closer to the NH_3 and OH_2 ligands, as shown by the spatial distribution function (SDF) in Fig. 3. The SDF can be thought of as a three-dimensional generalization of an RDF. The SDF isosurfaces indicate the regions in space where the relevant probability density exceeds the density averaged over simulation box.

A. Dynamics in solution

To evaluate the dynamics of the complexes in solution, the geometrical parameters shown in Fig. 4 were probed. The histograms for the dihedral angle distributions, O_{12}–Pt_2–Pt_1–N_{31} and O_{22}–Pt_2–Pt_1–N_{41}, and the evolution in time of the Pt–L distances

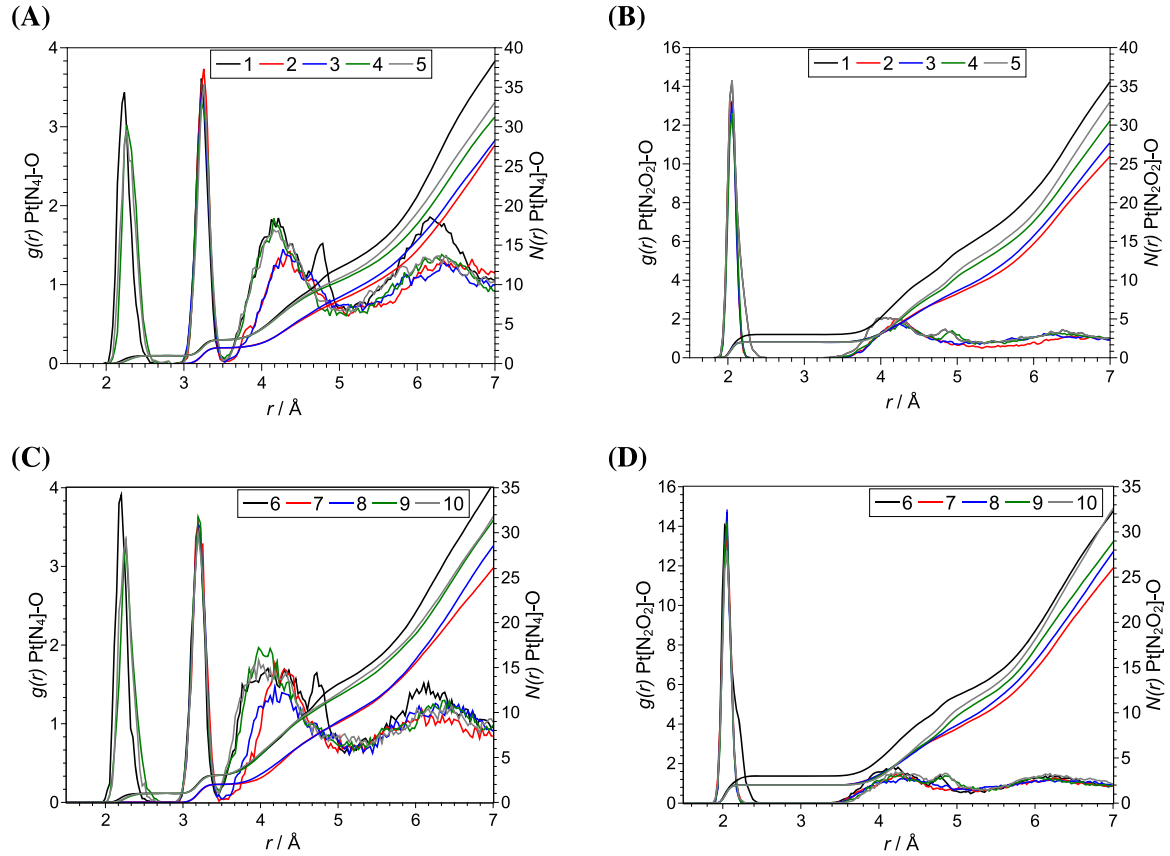

FIG. 2. Platinum–oxygen RDFs, $g(r)$[Pt–O] (left vertical axes), and the corresponding radial integrals, $N(r)$[Pt–O] (right vertical axes), for the ten platinum complexes. (A) and (B): α–pyrrolidonate-bridged complexes. (C) and (D): Pivalamidate-bridged complexes.

are shown in Figs. S6 and S7, respectively. Rotations around the Pt–Pt bond are obviously hindered by the bridging ligands, restricting the dihedral angle ranges to the range of approximately −30° to +30°. The diaquo and dihalo α–pyrrolidonate-bridged complexes (**1**, **4**, and **5**) presented a twisted conformational preference. The aforementioned dihedral angles have their highest probability to be around −5° and 12° for diaquo and dihalo complexes, respectively. The aquahalo complexes (**2** and **3**) exhibit dihedral angles that are more evenly distributed, i.e., the hindered rotation around the Pt–Pt bond occurs somewhat more easily.

For the pivalamidate-bridged complexes (**6**–**10**) the rotation around Pt–Pt is similar to those in the α–pyrrolidonate-bridged systems. The α-pyridonate-bridged complexes demonstrate a higher probability of torsional angles around 22° and 25°, which suggest a twisted conformation for those with diaquo and aquahalo axial ligands, respectively. In contrast, complexes with dihalo axial-substituted ligands exhibit angles ranging between −5° and −30°.[36] In comparison to structurally analogous bridging complexes, acetate-bridged Pt^{III} compounds with dihalo (Br^- and Cl^-) axial ligands exhibit small torsion angles, less than 5.5°, yielding eclipsed conformations.[86] Conversely, carboxylate-bridged complexes with *cis*-methyl groups instead of amines exhibit larger angles around 22°–25°.[87,88] Hence, the variations in the rotation around the Pt–Pt bond are likely not only solely attributed to the bridging ligands but also influenced by the nature of the axial ligands. However, it was observed that the angle formed by the N– C– O atoms from the bridging ligand is on average 125° for **1**–**5** and 121° for **6**–**10**. This suggests that the greater the angle of N–C–O, the greater the average bond length between Pt atoms, i.e., pivalamidate < α–pyrrolidonate, which could ease the rotation around that bond because the steric hindrance between NH_3 groups is reduced and the Pt–Pt bond becomes more labile.

The conformational preference of the complexes is related to the trans influence caused by the axial ligands and the bridging ligands as well.[36] The *trans* influence is responsible for changes in the Pt–L bond lengths since the Pt–L_1 distance varies as α–pyrrolidonate > pivalamidate, while the Pt–L_2 distance tends to increase in the opposite order. The complexes bridged by α-pyridonate demonstrate a Pt–L_1 value higher than the compounds studied in this work. Meanwhile, the P–L_2 value is observed to be lower in these complexes compared to the investigated compounds.[36] These structural features are crucial to ^{195}Pt NMR calculations and need to be taken into account to reach a good agreement between the experimental and theoretical data.[5]

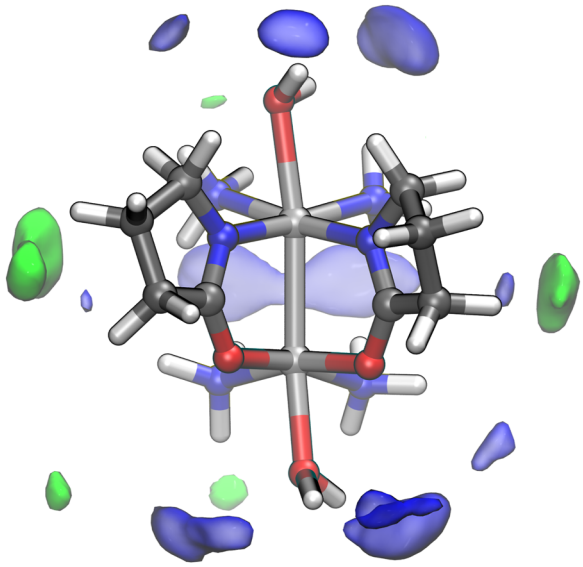

FIG. 3. Spatial distribution function (SDF) showing the regions of high probability for finding water molecules (blue color) and the perchlorate ions (green color) surrounding complex 1. The SDF was generated by the TRAVIS program[84,85] and visualized by VMD[68] with isovalue for each surface of 145.1 (H_2O) and 75.9 (ClO_4^-), respectively.

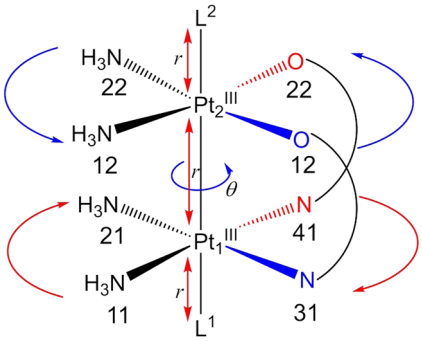

FIG. 4. Schematic representation of the geometrical parameters evaluated to probe the dynamics of the complexes in solution: distances Pt–Pt, Pt_1–L_1, and Pt_2–L_2. Dihedral angles O_{12}–Pt_2–Pt_1–N_{31} (blue) and O_{22}–Pt_2–Pt_1–N_{41} (red).

B. Static vs dynamic complexes' treatment on $^1J_{PtPt}$

The computed *J*–coupling constants were evaluated by employing static and dynamic approaches with and without solvation, employing the models presented in Table II. In the models Static^{bare} and Static^{COSMO}, a *static* optimized geometry with and without implicit solvation (continuum model) is considered, respectively. In the AIMD^{bare} model, all solvent molecules were stripped off the AIMD configurations. NMR parameters were subsequently calculated for the "bare" un-solvated complexes and averaged along the trajectories. The full AIMD model (AIMD^{Full}) includes explicit microsolvation and the continuum model to describe the bulk solvent effects. As discussed previously, the AIMD model indicated that the complexes have ten solvent molecules (counting solvent proper and counter ions) in the first shell. Table S1 in the supplementary material presents the average composition and the charge of each cluster evaluated. This is supported by extensive NMR test calculations, detailed in Sec. S2 in the supplementary material, showing that the $^1J_{PtPt}$ data in the full AIMD model are converged when $N = 10$ explicit solvent molecules are included in the NMR calculations. The following discussion is based on the calculations with $N = 10$.

For diaqua complexes (**1** and **6**), the Static^{COSMO} and AIMD^{bare} models provided results that were, on average, 7.0 and 5.9 kHz, respectively, lower than the Static^{bare} model. Relative to Static^{bare}, the Static^{COSMO} model only gives the static electrostatic contribution from the solute electron density polarization to the direct solvent effect, whereas the AIMD^{bare} model produces only the indirect solvent effect in the dynamic setup.[7,8] Our results indicate that the inclusion of both these effects is very important to produce accurate $^1J_{PtPt}$. Accordingly, even more accurate $^1J_{PtPt}$ are obtained when both explicit and implicit solvations are applied to the *dynamic* configurations (AIMD^{Full} model), with results that are, on average, about 2.9 kHz lower than the AIMD^{bare} model. However, the full AIMD results remain noticeably higher than the experimental $^1J_{PtPt}$, even though they are strongly improved over the other models.

For the dihalo and aquahalo complexes, the implicit solvation on the static geometries, on average, increases $^1J_{PtPt}$ by 3.1 and 3.9 kHz, respectively. The results of the AIMD^{bare} model have a slightly greater deviation from the experimental data compared to the Static^{bare} model except for those in complex **5**. In the AIMD^{Full} model, where electrostatic, dynamic, and explicit solvent contributions are considered, $^1J_{PtPt}$ does not change significantly in comparison to the Static^{COSMO} model [see points 5–25 of Figs. S2(a) and S2(b)], showing a small net contribution of solute–solvent interactions. The final AIMD $^1J_{PtPt}$ values calculated by means of the AIMD^{Full} regime are overestimated by 3.2 ± 0.4 kHz, on average, when compared to the experiments. For the α-pyridonate-bridged complexes,[36] similar trends were observed for the calculated *J*-coupling. However, the $^1J_{PtPt}$ experimental trend: diaqua > aquachloro > aquabromo > dichloro > dibromo is reproduced by the calculations for the α–pyrrolidonate-bridged complexes. For the pivalamidate-bridged complexes, the experimental trend was mostly reproduced with the exception of a swap between aquabromo and aquachloro, whose $^1J_{PtPt}$ values differ only by 168 Hz, similar to that observed for the α-pyridonate-bridged systems.

The correlation between experimental and theoretical data, shown in Fig. 5, provides a comprehensive assessment of the accuracy of the evaluated static and dynamic models. Despite a slight overestimation of the experimental data, the AIMD^{Full} model stands out, showing the highest correlation and indicating a more consistent estimate of the *J*-coupling. Moreover, it is important to point out that the accuracy of the electronic structure method used here has previously been estimated to give around 13% median percentage errors with respect to experimental data,[57] which has been confirmed by some of our previous work.[7,12,20,36,89] Concerning the structural changes of the complexes in solution, including the Pt–Pt and Pt–L bond lengths, dihedral angles, and the different bridging ligands, no direct correlation was identified between them and the $^1J_{PtPt}$ values. This stems from the AIMD simulations revealing that

TABLE II. Calculated vs experimental $^1J_{PtPt}$ coupling constants[a] for α–pyrrolidonate- (**1–5**) and pivalamidate-bridged (**6–10**) complexes. Calculations with different solvated and unsolvated models.

Complex	L^1/L^2	Static^{bare}[b]	Static^{COSMO}[c]	AIMD^{bare}[d]	AIMD^{Full}[e]	Expt.[f]
1	H_2O/H_2O	22 245 [135]	15 644 [65]	15 301 [61]	12 836 [35] (12 659)	9482
2	Br^-/Br^-	7267 [9]	10 917 [63]	5329 [−20]	9629 [44] (9633)	6682
3	Cl^-/Cl^-	6566 [−8]	9721 [36]	5883 [−18]	10 334 [45] (10 428)	7132
4	Br^-/H_2O	7208 [−9]	12 353 [56]	6866 [−14]	11 373 [43] (11 790)	7940
5	Cl^-/H_2O	6731 [−17]	11 701 [45]	7657 [−5]	11 829 [46] (12 014)	8096
6	H_2O/H_2O	21 067 [127]	13 666 [48]	16 266 [76]	12 974 [40] (12 947)	9262
7	Br^-/Br^-	6332 [−8]	9084 [32]	5653 [−18]	9866 [43] (9800)	6902
8	Cl^-/Cl^-	6625 [−8]	9438 [31]	6181 [-−14]	9970 [38] (9969)	7216
9	Br^-/H_2O	7566 [−6]	10 821 [34]	6679 [−17]	11 078 [37] (11 153)	8086
10	Cl^-/H_2O	8455 [3]	10 883 [32]	7579 [−8]	10 910 [32] (11 078)	8234
1^{HH}[g]	H_2O/H_2O	19 971 [125]	18 843 [112]	15 037 [69]	11 633 [31] (11 629)	8886
2^{HH}[g]	Br^-/Br^-	5578 [−12]	7921 [26]	5140 [−18]	8680 [38] (8553)	6306
3^{HH}[g]	Cl^-/Cl^-	5922 [−11]	8285 [25]	5574 [−16]	9275 [40] (9236)	6636
4^{HH}[g]	Br^-/H_2O	7358 [−3]	9694 [28]	6561 [−13]	10 520 [39] (10 558)	7574
5^{HH}[g]	Cl^-/H_2O	7649 [−2]	10 752 [38]	6686 [−14]	10 413 [34] (10 328)	7774

[a]Results are in units of Hz. The calculations were performed with PBE0/ZORA SO/TZP(jcpl). The values in the square brackets are the relative deviation in percent with respect to the experimental data. The standard errors for each average value for AIMD^{bare} and AIMD models are presented in Table S2.
[b]Unsolvated optimized geometry and no solvation used in NMR calculation.
[c]Geometry optimization and NMR calculation with the implicit solvation model.
[d]Arithmetic average of 64 AIMD configurations, using only the solute. No solvation included.
[e]Arithmetic average of 256 AIMD configurations, each including ten explicit nearest-neighbor solvent molecules (or counter ions) and added implicit solvation model to treat bulk effects. The values in parentheses represent the average of the 64 AIMD configurations used for the AIMD^{bare} column.
[f]Measurements using an acidic D_2O solution ($DClO4/D_2O$) to suppress the deprotonation of diaqua complexes. Data extracted from Ref. 39.
[g]α-pyridonate-bridged complexes, Ref. 36.

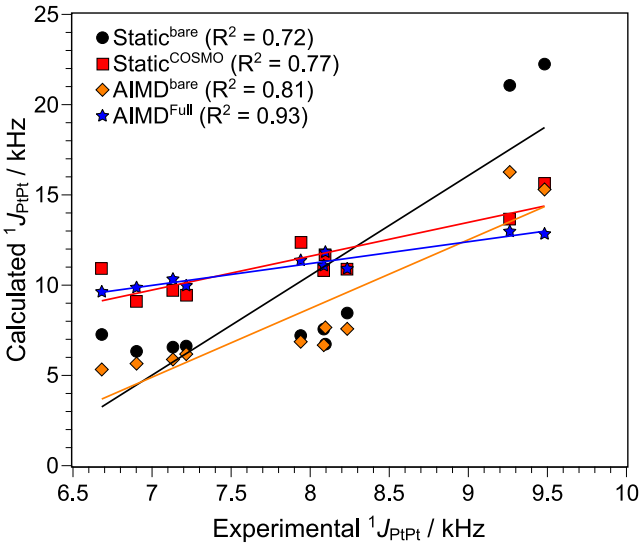

FIG. 5. Correlation between experimental and calculated NMR $^1J_{PtPt}$ for the different computational models. The lines correspond to the linear regressions for the datasets of each evaluated system setup.

geometric effects are notably pronounced, given simultaneous variations in multiple bond lengths and/or dihedral angles (Sec. III A). Thus, the trends in *J*-coupling observed among complexes with the different bridging ligands α-pyridonate,[36] α–pyrrolidonate, and pivalamidate, but identical axial ones highlight the contrasting chemical environments experienced by the L_1–Pt_1–Pt_2–L_2 backbone. These differences in the chemical environment lead to a polarization of the Pt–Pt bond (such as $L_1-Pt_1^{II}-Pt_2^{IV}-L_2$), which is affected by both the equatorial ligands[39,47,90] and the axial ligands.[36,91] As a result, several effects, such as geometrical, electronic, substituent, and solvation, collectively contribute to the experimental and calculated the $^1J_{PtPt}$ range.

C. Contributions to $^1J_{PtPt}$ in the dynamic approach

Each effect present in the dynamic treatment was isolated to better understand its contribution to the total $^1J_{PtPt}$ value, based on Eqs. (1a)–(1d). Here, J^{vib} corresponds to the nuclear motion (mostly of vibrational nature) during the dynamics. Effects from implicit solvation are denoted by $J^{solv,impl}$, explicit solvation effects are denoted as $J^{solv,expl}$, and bulk solvation by $J^{solv,bulk}$.

$$J^{\mathrm{vib}} = \mathrm{AIMD}^{\mathrm{bare}} - \mathrm{Static}^{\mathrm{bare}}, \tag{1a}$$

$$J^{\mathrm{solv,impl}} = \mathrm{AIMD}_{0\mathrm{NN}}^{\mathrm{COSMO}} - \mathrm{AIMD}^{\mathrm{bare}}, \tag{1b}$$

$$J^{\mathrm{solv,expl}} = \mathrm{AIMD}^{10\mathrm{NN}} - \mathrm{AIMD}^{\mathrm{bare}}, \tag{1c}$$

$$J^{\mathrm{solv,bulk}} = \mathrm{AIMD}^{\mathrm{Full}} - \mathrm{AIMD}^{10\mathrm{NN}}. \tag{1d}$$

It is worth mentioning that the sum of $^1J_{\mathrm{PtPt}}$ obtained from the Static$^{\mathrm{bare}}$ model combined with J^{vib}, $J^{\mathrm{solv,expl}}$, and $J^{\mathrm{solv,bulk}}$ is equal to the J-coupling calculated using the full AIMD model [referred to as AIMD$^{\mathrm{Full}}$ in Eq. (1d)]. Here, $^1J_{\mathrm{PtPt}}$ was calculated using the AIMD configurations solvated by 10NN solvent molecules without COSMO specifically to isolate the explicit solvation. $J^{\mathrm{solv,impl}}$ is the solvent effect in the dynamic model that would be obtained using only COSMO, without additional microsolvation. This contribution is not equal to $J^{\mathrm{solv,bulk}}$ because the solvent-accessible surface generated for the continuum model surrounds the complex with its first explicit solvation shell in the latter case (bulk), whereas the surface directly interacts with the solute complex in the calculation, labeled AIMD$_{0\mathrm{NN}}^{\mathrm{COSMO}}$.

The partitioning in equation set (1) was performed for a subset of the systems. The results are presented graphically in Fig. 6. For the diaqua complexes, all contributions to $^1J_{\mathrm{PtPt}}$, arising from the dynamics and solvation are negative and reduce the J-coupling magnitude. The dynamic conformational treatment (reflected in J^{vib}) and the inclusion of explicit solvent molecules ($J^{\mathrm{solv,expl}}$) together

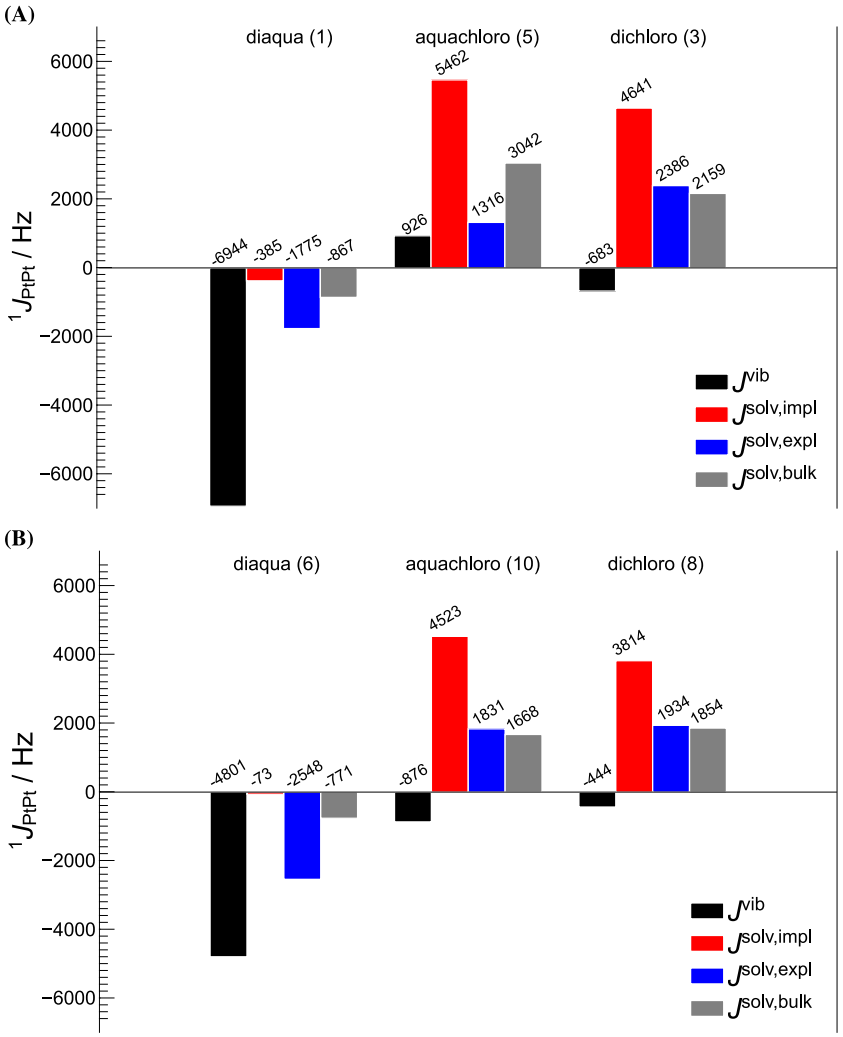

FIG. 6. Contributions from nuclear motion (J^{vib}), implicit solvation ($J^{\mathrm{solv,impl}}$), explicit solvation ($J^{\mathrm{solv,expl}}$), and bulk solvent effect ($J^{\mathrm{solv,bulk}}$) for $^1J_{\mathrm{PtPt}}$ of the diaqua, aquachloro, and dichloro complexes with bridging α–pyrrolidonate (a) and pivalamidate (b) ligands. See Eq. (1). All data are arithmetically averaged over 64 AIMD configurations and include SO effects.

with the bulk effects are evidently of great importance for an accurate description of the coupling. The higher magnitude of $J^{solv,expl}$ compared to $J^{solv,bulk}$ for these complexes is related to solute–solvent interactions mediated via hydrogen bonds of the axial aqua ligands. Visual inspection of the simulations revealed that the hydrogen bond interactions along with the exchange of aqua ligands and solvent water molecules are also responsible for changes in the solute structure throughout the dynamics. In turn, this causes a pronounced indirect solvent effect, which is reflected in a large J^{vib} contribution.

For the analyzed aquachloro and dichloro complexes, $J^{solv,impl}$, $J^{solv,expl}$, and $J^{solv,bulk}$ each increases the total coupling with respect to the Static^{bare} model, while a small negative J^{vib} is found for compounds **3**, **8**, and **10**. The positive J^{vib} for complex **5** can be explained by the more pronounced rotation around the Pt–Pt bond caused by the larger angle N–C–O of the bridged group, as mentioned in Sec. III A.

The large $J^{solv,impl}$ for the aquachloro and dichloro complexes shows that COSMO polarization is more effective on complexes containing axial halogens. In the aquahalo complex, $J^{solv,impl}$ is almost 800 Hz greater than in the dihalo complex. The reason for this is that the metal–metal bond tends to be easily polarizable in the aquahalo complex because the system has the Pt^{IV}–Pt^{II} character.[36,39] It is interesting to note that the $J^{solv,impl}$ contributions are close to the sum of $J^{solv,expl}$ and $J^{solv,bulk}$, which may lead to a misleading interpretation of the solvation effects if they are only determined with the help of a model such as COSMO.

Regarding geometric parameters, such as the Pt–Pt and Pt–L distances as well as the dihedral angles, no direct relationship was found between the change of a single parameter and the trends in $^1J_{PtPt}$. The use of AIMD shows that the variations in the bond lengths and dihedral angles are pronounced. These variations go along with complex changes in the electronic structure that are reflected in the calculated J-coupling via the J^{vib} contribution, that is, the indirect solvent effect.

D. Treatment of relativistic effects

As previously shown for α-pyridonate-bridged complexes,[36] and also for the complexes investigated here, the calculations based on 2c-ZKS lead to overestimated $^1J_{PtPt}$ values. Then, the question arises whether this overestimation is caused by the approximations inherent in ZORA or by other approximations that are made in the calculations. To evaluate the accuracy of the relativistic treatment, $^1J_{PtPt}$ of the diaqua complexes was also calculated using 4c-DKS with the same underlying PBE0 hybrid functional. The results are summarized in Table III.

For all models, the results show that the calculated $^1J_{PtPt}$ value is larger with 4c-DKS than it is in the 2c-ZKS calculations, and therefore, 4c-DKS overestimates the experimental values even more strongly. It is important to note that the difference in the results ($\Delta_{ZKS\text{-}DKS}$) between the two relativistic Hamiltonians decreases as the model is improved. The difference becomes insignificant for the explicitly solvated systems when considering the overall agreement with the experimental data. The effect of the dynamic treatment, and more so of the microsolvation, is somewhat unintuitive because the relativistic effects and differences between quasi- relativistic and fully relativistic Hamiltonians are expected to be mainly associated with the atomic core regions. We tentatively assign the sizable differences between 2c-ZKS and 4c-DKS for the "bare" model systems as being associated with the diffuse regions of the molecule. Here, the differences between the basis set types in the two sets of calculations, namely, STOs in 2c-ZKS vs GTOs in the 4c-DKS calculations, potentially play an important role. Once the systems are solvated with explicit water molecules, the properties of the solute will be modified by the presence of the microsolvation shell, as previously shown,[12] and therefore, the differences in the description of the diffuse molecular regions via the long-range behavior of the AO basis set will be less important than in the gas phase. Furthermore, when the results without and with microsolvation are compared for 64 individual AIMD configurations (see Tables S4 and S5), it is clear that most of the differences between the J-coupling obtained from 2c-ZKS and 4c-DKS not only become insignificant for the AIMD average but also for each individual AIMD configuration.

TABLE III. Comparison between $^1J_{PtPt}$ of diaqua complexes calculated with 2c-ZKS and 4c-DKS Hamiltonians arithmetically averaged over 64 AIMD configurations.[a]

	2c-ZKS		4c-DKS		$\Delta_{ZKS\text{-}DKS}$	
Model	1	6	1	6	1	6
Static^{Bare}	22 245	21 067	24 896	23 158	−2651	−2091
AIMD^{Bare}	15 301	16 266	16 625	17 567	−1324	−1301
AIMD^{10NN}	13 525	13 718	13 745	13 980	−220	−262
AIMD^{Full}	12 659	12 947	12 878[b]	13 209[b]	−219	−262

[a]Results are in units of Hz. The standard errors for each average value for the 4c-DKS models are presented in Table S3.
[b]Due to the absence of COSMO in the Respect program, the model AIMD^{10NN} in 4c-DKS calculations was adjusted by adding the $J^{solv,bulk}$ contribution from 2c-ZKS calculations.

Therefore, as shown previously in the literature,[19,24,25,32–35] for compounds containing heavy elements and properties that are determined by valence-shell orbitals, such as NMR shifts and J-couplings, the 2c-ZKS Hamiltonian is accurate. Likewise, in the present study, essentially the same deviations between theory and experiment are found in the dynamic calculations with microsolvation when using 2c-ZKS or 4c-DKS. It is likely that systematic improvements will be obtained only when the electronic structure treatment and the dynamic sampling are further improved simultaneously. Wilson and Lipard[86] also had difficulties in obtaining good results for the Pt–Pt bond length, which is related to the fact that DFT functionals have difficulties in elucidating weak d_8–d_8 interactions in Pt(II) complexes.[92] Thus, we suggest that the next step to improve the accuracy of the calculated NMR parameters for these Pt(III) complexes would be the adoption of a hybrid functional in the AIMD simulations to reduce errors in the description of geometric parameters; as well as a larger sampling through longer simulations. However, this still remains a challenge given the high computational cost of AIMD.

IV. CONCLUSIONS

In the present work, we elucidated the dynamic solvent effect on the $^1J_{PtPt}$ coupling constants of α–pyrrolidonate- and

pivalamidate-bridged Pt^{III} dinuclear complex derivatives through AIMD simulations and NMR calculations with two-component and four-component relativistic treatments.

The decomposition of the total J-coupling into different contributions from the dynamic treatment showed that, for diaquo complexes, they all lead to a reduction, while for the dihalo and aquahalo complexes, most of these contributions lead to an increase in the coupling. The diaquo complexes were the most sensitive to the effects of dynamic treatment, in which the vibrational (J^{vib}) and the explicit solvation ($J^{solv,exp}$) contributions are responsible for reducing the J-coupling of the diaquo complexes by ~8 kHz. For the dihalo and aquahalo complexes, implicit solvation ($J^{solv,imp}$) and bulk solvation ($J^{solv,bulk}$) are the most important contributions. The former accurately reproduces the solvent on the AIMD configurations when the explicit solvent molecules are removed, while the latter has almost the same contribution to J-coupling as the explicit solvation in the $AIMD^{Full}$ model. These findings show that configuration sampling through a dynamic approach and explicit treatment of at least the first solvent shell, along with the bulk solvent effects, are highly relevant to get a complete and more accurate description of the NMR tensors of the investigated complexes.

The relativistic treatment based on a quasirelativistic vs a fully relativistic Hamiltonian yields overestimated $^1J_{PtPt}$ with essentially the same deviations from the experimental data. Therefore, the approximate treatment of relativity by ZORA is unlikely to be the major source of errors. The observed deviations between the calculated and measured NMR data most likely arise from other approximations used for the molecular dynamics and the NMR calculations, such as finite configuration sampling, finite basis errors, and the DFT approximations used in the dynamics and in the electronic structure calculations for the NMR parameters.

SUPPLEMENTARY MATERIAL

The supplementary material provides details on assessment of molecular dynamics, solvent effect on the $^1J_{PtPt}$ coupling, configuration sampling, structural characterization of complexes in solution, and errors of the average J-value.

ACKNOWLEDGMENTS

We acknowledge the National Laboratory for Scientific Computing (LNCC/MCTI, Brazil, SDumont supercomputer) and the Center for Computational Research (CCR) of the University at Buffalo for providing high performance computing resources. L.C.D. and P.R.B. acknowledge Grant Nos. 2017/17750-3 and 2018/07308-4 from the São Paulo Research Foundation (FAPESP). L.C.D. also acknowledges CNPq Grant No. 306844/2020-6. J.A. acknowledges the support provided by the United States Department of Energy, Office of Science, Basic Energy Sciences (BES), Materials Chemistry program (Award No. DE-SC0022310).

AUTHOR DECLARATIONS

Conflict of Interest

The authors have no conflicts to disclose.

Author Contributions

Patrick R. Batista: Writing – original draft (equal). **Lucas C. Ducati**: Writing – review & editing (equal). **Jochen Autschbach**: Writing – review & editing (equal).

DATA AVAILABILITY

The data that support the findings of this study are available from the corresponding author upon reasonable request.

REFERENCES

[1] P. S. Pregosin, "Platinum-195 nuclear magnetic resonance," Coord. Chem. Rev. **44**, 247–291 (1982).
[2] P. S. Pregosin, "Platinum NMR spectroscopy," Annu. Rep. NMR Spectrosc. **17**, 285–349 (1986).
[3] B. M. Still, P. G. A. Kumar, J. R. Aldrich-Wright, and W. S. Price, "^{195}Pt NMR—Theory and application," Chem. Soc. Rev. **36**, 665–686 (2007).
[4] J. Autschbach and S. Zheng, "Relativistic computations of NMR parameters from first principles: Theory and applications," Annu. Rep. NMR Spectrosc. **67**, 1–95 (2009).
[5] M. Sterzel and J. Autschbach, "Toward an accurate determination of ^{195}Pt chemical shifts by density functional computations: The importance of unspecific solvent effects and the dependence of Pt magnetic shielding constants on structural parameters," Inorg. Chem. **45**, 3316–3324 (2006).
[6] J. Autschbach and S. Zheng, "Analyzing Pt chemical shifts calculated from relativistic density functional theory using localized orbitals: The role of Pt 5d lone pairs," Magn. Reson. Chem. **46**, S45–S55 (2008).
[7] L. A. Truflandier and J. Autschbach, "Probing the solvent shell with ^{195}Pt chemical shifts: Density functional theory molecular dynamics study of Pt^{II} and Pt^{IV} anionic complexes in aqueous solution," J. Am. Chem. Soc. **132**, 3472–3483 (2010).
[8] L. A. Truflandier, K. Sutter, and J. Autschbach, "Solvent effects and dynamic averaging of the ^{195}Pt NMR shielding in cisplatin derivatives," Inorg. Chem. **50**, 1723–1732 (2011).
[9] K. Sutter, L. A. Truflandier, and J. Autschbach, "NMR J–coupling constants in cisplatin derivatives studied by molecular dynamics and relativistic DFT," ChemPhysChem **12**, 1448–1455 (2011).
[10] J. C. Davis, M. Bühl, and K. R. Koch, "On the origin of $^{35/37}$Cl isotope effects on ^{195}Pt NMR chemical shifts. A density functional study," J. Chem. Theory Comput. **8**, 1344–1350 (2012).
[11] B. E. G. Lucier, K. E. Johnston, W. Xu, J. C. Hanson, S. D. Senanayake, S. Yao, M. W. Bourassa, M. Srebro, J. Autschbach, and R. W. Schurko, "Unravelling the structure of Magnus' pink salt," J. Am. Chem. Soc. **136**, 1333–1351 (2014).
[12] L. C. Ducati, A. Marchenko, and J. Autschbach, "NMR J-coupling constants of Tl–Pt bonded metal complexes in aqueous solution: Ab-initio molecular dynamics and localized orbital analysis," Inorg. Chem. **55**, 12011–12023 (2016).
[13] A. C. Castro, H. Fliegl, M. Cascella, T. Helgaker, M. Repisky, S. Komorovsky, M. Á. Medrano, A. G. Quiroga, and M. Swart, "Four-component relativistic ^{31}P NMR calculations for *trans*-platinum(ii) complexes: Importance of the solvent and dynamics in spectral simulations," Dalton Trans. **48**, 8076–8083 (2019).
[14] A. H. Mazurek, Ł. Szeleszczuk, and D. M. Pisklak, "A review on combination of ab initio molecular dynamics and NMR parameters calculations," Int. J. Mol. Sci. **22**, 4378 (2021).
[15] M. Bühl and F. T. Mauschick, "Thermal and solvent effects on ^{57}Fe NMR chemical shifts," Phys. Chem. Chem. Phys. **4**, 5508–5514 (2002).
[16] T. M. Alam, D. Hart, and S. L. B. Rempe, "Computing the ^{7}Li NMR chemical shielding of hydrated Li^+ using cluster calculations and time-averaged configurations from *ab initio* molecular dynamics simulations," Phys. Chem. Chem. Phys. **13**, 13629–13637 (2011).
[17] M. Dračínský, H. M. Möller, and T. E. Exner, "Conformational sampling by ab initio molecular dynamics simulations improves NMR chemical shift predictions," J. Chem. Theory Comput. **9**, 3806–3815 (2013).

[18]L. Halbert, M. Olejniczak, V. Vallet, and A. Severo Pereira Gomes, "Investigating solvent effects on the magnetic properties of molybdate ions (MoO_4^{2-}) with relativistic embedding," Int. J. Quantum Chem. **120**, e26207 (2019).
[19]A. C. Castro, D. Balcells, M. Repisky, T. Helgaker, and M. Cascella, "First-principles calculation of ^{1}H NMR chemical shifts of complex metal polyhydrides: The essential inclusion of relativity and dynamics," Inorg. Chem. **59**, 17509–17518 (2020).
[20]L. A. Schenberg, L. C. Ducati, and J. Autschbach, "Inquiring ^{199}Hg NMR parameters by combining ab initio molecular dynamics and relativistic NMR calculations," Inorg. Chem. **63**, 2082 (2024).
[21]Y. Xiao, W. Liu, and J. Autschbach, "Relativistic theories of NMR shielding," in *Handbook of Relativistic Quantum Chemistry*, edited by W. Liu (Springer, Berlin, 2017), pp. 657–692.
[22]J. Autschbach, "Relativistic effects on NMR parameters," in *High Resolution Nuclear Magnetic Resonance Parameters for Understanding Molecules and their Electronic Structure*, edited by R. H. Contreras (Elsevier, Amsterdam, 2013), Vol. 3, pp. 69–117.
[23]E. van Lenthe and E. Jan Baerends, "Density functional calculations of nuclear quadrupole coupling constants in the zero-order regular approximation for relativistic effects," J. Chem. Phys. **112**, 8279–8292 (2000).
[24]J. Autschbach, "The accuracy of hyperfine integrals in relativistic NMR computations based on the zeroth-order regular approximation," Theor. Chem. Acc. **112**, 52–57 (2004).
[25]J. Autschbach, "The role of the exchange-correlation response kernel and scaling corrections in relativistic density functional nuclear magnetic shielding calculations with the zeroth-order regular approximation," Mol. Phys. **111**, 2544–2554 (2013).
[26]R. Narayanan, M. Nakada, M. Abe, M. Saito, and M. Hada, "^{13}C and ^{207}Pb NMR chemical shifts of dirhodio- and dilithioplumbole complexes: A quantum chemical assessment," Inorg. Chem. **58**, 14708–14719 (2019).
[27]H. Dossmann, D. Gatineau, H. Clavier, A. Memboeuf, D. Lesage, and Y. Gimbert, "Exploring phosphine electronic effects on molybdenum complexes: A combined photoelectron spectroscopy and energy decomposition analysis study," J. Phys. Chem. A **124**, 8753–8765 (2020).
[28]I. L. Rusakova and Y. Y. Rusakov, "Quantum chemical calculations of ^{77}Se and ^{125}Te nuclear magnetic resonance spectral parameters and their structural applications," Magn. Reson. Chem. **59**, 359–407 (2021).
[29]A. Berkefeld, M. Reimann, G. Hörner, M. Kaupp, and H. Schubert, "C–P vs C–H bond cleavage of triphenylphosphine at platinum(0): Mechanism of formation, reactivity, redox chemistry, and NMR chemical shift calculations of a μ-phosphanido diplatinum(II) platform," Organometallics **39**, 443–452 (2020).
[30]I. V. Mirzaeva, "Large relativistic effects in ^{119}Sn NMR parameters: A case study of complex anions $[Cp^*M(SnCl_3)_nCl_{3-n}]^-$, where M = Rh, Ir; n = 1, 2, 3," Comput. Theor. Chem. **1205**, 113432 (2021).
[31]F. P. Caló, G. Bistoni, A. A. Auer, M. Leutzsch, and A. Fürstner, "Triple resonance experiments for the rapid detection of ^{103}Rh NMR shifts: A combined experimental and theoretical study into dirhodium and bismuth–rhodium paddlewheel complexes," J. Am. Chem. Soc. **143**, 12473–12479 (2021).
[32]V. Arcisauskaite, J. I. Melo, L. Hemmingsen, and S. P. A. Sauer, "Nuclear magnetic resonance shielding constants and chemical shifts in linear ^{199}Hg compounds: A comparison of three relativistic computational methods," J. Chem. Phys. **135**, 044306 (2011).
[33]A. Wodynski, M. Repisky, and M. Pecul, "A comparison of two-component and four-component approaches for calculations of spin-spin coupling constants and NMR shielding constants of transition metal cyanides," J. Chem. Phys. **137**(1), 014311 (2012).
[34]J. Vícha, J. Novotný, M. Straka, M. Repisky, K. Ruud, S. Komorovsky, and R. Marek, "Structure, solvent, and relativistic effects on the NMR chemical shifts in square-planar transition-metal complexes: Assessment of DFT approaches," Phys. Chem. Chem. Phys. **17**, 24944–24955 (2015).
[35]S. Komorovsky, K. Jakubowska, P. Świder, M. Repisky, and M. Jaszuński, "NMR spin–spin coupling constants derived from relativistic four-component DFT theory–analysis and visualization," J. Phys. Chem. A **124**, 5157–5169 (2020).
[36]P. R. Batista, L. C. Ducati, and J. Autschbach, "Solvent effect on the ^{195}Pt NMR properties in pyridonate-bridged Pt^{III} dinuclear complex derivatives by *ab initio* molecular dynamics and localized orbital analysis," Phys. Chem. Chem. Phys. **23**, 12864–12880 (2021).
[37]A. Fernández-Alarcón and J. Autschbach, "Relativistic density functional NMR tensors analyzed with spin-free localized molecular orbitals," ChemPhysChem **24**, e202200667 (2023).
[38]J. D. Woollins and P. F. Kelly, "The preparation and properties of compounds containing Pt(III)," Coord. Chem. Rev. **65**, 115–140 (1985).
[39]S. Iwatsuki, E. Isomura, A. Wada, K. Ishihara, and K. Matsumoto, "^{195}Pt NMR spectra of head-to-head and head-to-tail amidato-bridged platinum(III) dinuclear complexes," Eur. J. Inorg. Chem. **2006**, 2484–2490.
[40]B. Rosenberg, L. Van Camp, and T. Krigas, "Inhibition of cell division in *Escherichia coli* by electrolysis products from a platinum electrode," Nature **205**, 698–699 (1965).
[41]B. Rosenberg, L. Vancamp, J. E. Trosko, and V. H. Mansour, "Platinum compounds: A new class of potent antitumour agents," Nature **222**, 385–386 (1969).
[42]B. Rosenberg and L. VanCamp, "The successful regression of large solid sarcoma 180 tumors by platinum compounds," Cancer Res. **30**, 1799–1802 (1970).
[43]S. J. Lippard, "New chemistry of an old molecule: *cis*-$[Pt(NH_3)_2Cl_2]$," Science **218**, 1075–1082 (1982).
[44]M. Yoshida, N. Yashiro, H. Shitama, A. Kobayashi, and M. Kato, "A redox-active dinuclear platinum complex exhibiting multicolored electrochromism and luminescence," Chem. - Eur. J. **22**, 491–495 (2016).
[45]A. Stiegman, V. Miskowski, and H. B. Gray, "Metal-metal excited-state emission from binuclear platinum(III) complexes," J. Am. Chem. Soc. **108**, 2781–2782 (1986).
[46]T. M. Swager, "The molecular wire approach to sensory signal amplification," Acc. Chem. Res. **31**, 201–207 (1998).
[47]K. Matsumoto and K. Sakai, "Structures and reactivities of platinum-blues and the related amidate bridged platinum(III) compounds," Adv. Inorg. Chem. **49**, 375–427 (2000).
[48]M. A. Bennett, S. K. Bhargava, E. C.-C. Cheng, W. H. Lam, T. K.-M. Lee, S. H. Privér, J. Wagler, A. C. Willis, and V. W.-W. Yam, "Unprecedented near-infrared (NIR) emission in diplatinum(III) (d^7–d^7) complexes at room temperature," J. Am. Chem. Soc. **132**, 7094–7103 (2010).
[49]X. Wu *et al.*, "Highly emissive dinuclear platinum(III) complexes," J. Am. Chem. Soc. **142**, 7469–7479 (2020).
[50]M. Xue, T.-L. Lam, G. Cheng, W. Liu, K.-H. Low, L. Du, S. Xu, F.-F. Hung, D. L. Phillips, and C.-M. Che, "Exceedingly stable luminescent dinuclear Pt(II) complexes with ditopic formamidinate bridging ligands for high-performance red and deep-red OLEDs with LT_{97} up to 2446 h at 1000 cd m^{-2}," Adv. Opt. Mater. **10**, 2200741 (2022).
[51]P. Giannozzi, S. Baroni, N. Bonini, M. Calandra, R. Car, C. Cavazzoni, D. Ceresoli, G. L. Chiarotti, M. Cococcioni, I. Dabo, A. Dal Corso, S. de Gironcoli, S. Fabris, G. Fratesi, R. Gebauer, U. Gerstmann, C. Gougoussis, A. Kokalj, M. Lazzeri, L. Martin-Samos, N. Marzari, F. Mauri, R. Mazzarello, S. Paolini, A. Pasquarello, L. Paulatto, C. Sbraccia, S. Scandolo, G. Sclauzero, A. P. Seitsonen, A. Smogunov, P. Umari, and R. M. Wentzcovitch, "QUANTUM ESPRESSO: A modular and open-source software project for quantum simulations of materials," J. Phys.: Condens. Matter **21**, 395502 (2009).
[52]G. J. Martyna and M. E. Tuckerman, "A reciprocal space based method for treating long range interactions in *ab initio* and force-field-based calculations in clusters," J. Chem. Phys. **110**, 2810–2821 (1999).
[53]L. Martínez, R. Andrade, E. G. Birgin, and J. M. Martínez, "PACKMOL: A package for building initial configurations for molecular dynamics simulations," J. Comput. Chem. **30**, 2157–2164 (2009).
[54]J. M. Martínez and L. Martínez, "Packing optimization for automated generation of complex system's initial configurations for molecular dynamics and docking," J. Comput. Chem. **24**, 819–825 (2003).
[55]R. A. DiStasio, Jr., B. Santra, Z. Li, X. Wu, and R. Car, "The individual and collective effects of exact exchange and dispersion interactions on the *ab initio* structure of liquid water," J. Chem. Phys. **141**, 084502 (2014).
[56]J. P. Perdew, K. Burke, and M. Ernzerhof, "Generalized gradient approximation made simple," Phys. Rev. Lett. **77**, 3865–3868 (1996).

[57]S. Moncho and J. Autschbach, "Relativistic zeroth-order regular approximation combined with nonhybrid and hybrid density functional theory: Performance for NMR indirect nuclear spin–spin coupling in heavy metal compounds," J. Chem. Theory Comput. **6**, 223–234 (2010).
[58]A. Dal Corso, "Pseudopotentials periodic table: From H to Pu," Comput. Mater. Sci. **95**, 337–350 (2014).
[59]N. Troullier and J. Martins, "A straightforward method for generating soft transferable pseudopotentials," Solid State Commun. **74**, 613–616 (1990).
[60]R. Car and M. Parrinello, "Unified approach for molecular dynamics and density-functional theory," Phys. Rev. Lett. **55**, 2471–2474 (1985).
[61]M. E. Tuckerman and M. Parrinello, "Integrating the Car–Parrinello equations. I. Basic integration techniques," J. Chem. Phys. **101**, 1302 (1994).
[62]M. E. Tuckerman and M. Parrinello, "Integrating the Car–Parrinello equations. II. Multiple time scale techniques," J. Chem. Phys. **101**, 1316–1329 (1994).
[63]S. Grimme, "Do special noncovalent π–π stacking interactions really exist?," Angew. Chem., Int. Ed. **47**, 3430–3434 (2008).
[64]S. Nosé, "A unified formulation of the constant temperature molecular dynamics methods," J. Chem. Phys. **81**, 511 (1984).
[65]M. V. Fernández-Serra and E. Artacho, "Network equilibration and first-principles liquid water," J. Chem. Phys. **121**, 11136–11144 (2004).
[66]P. H.-L. Sit and N. Marzari, "Static and dynamical properties of heavy water at ambient conditions from first-principles molecular dynamics," J. Chem. Phys. **122**, 204510 (2005).
[67]H. S. Lee and M. E. Tuckerman, "Dynamical properties of liquid water from ab initio molecular dynamics performed in the complete basis set limit," J. Chem. Phys. **126**, 164501 (2007).
[68]W. Humphrey, A. Dalke, and K. Schulten, "VMD: Visual molecular dynamics," J. Mol. Graphics **14**, 33–38 (1996).
[69]B. G. Levine, J. E. Stone, and A. Kohlmeyer, "Fast analysis of molecular dynamics trajectories with graphics processing units—Radial distribution function histogramming," J. Comput. Phys. **230**, 3556–3569 (2011).
[70]J. Autschbach and T. Ziegler, "Nuclear spin-spin coupling constants from regular approximate relativistic density functional calculations. I. Formalism and scalar relativistic results for heavy metal compounds," J. Chem. Phys. **113**, 936–947 (2000).
[71]J. Autschbach and T. Ziegler, "Nuclear spin-spin coupling constants from regular approximate relativistic density functional calculations. II. Spin-orbit coupling effects and anisotropies," J. Chem. Phys. **113**, 9410–9418 (2000).
[72]J. Autschbach, "Two-component relativistic hybrid density functional computations of nuclear spin–spin coupling tensors using Slater–type basis sets and density–fitting techniques," J. Chem. Phys. **129**, 094105 (2008).
[73]E. J. Baerends, T. Ziegler, J. Autschbach, D. Bashford, A. Bérces, F. M. Bickelhaupt, C. Bo, P. M. Boerrigter, L. Cavallo, D. P. Chong, L. Deng, R. M. Dickson, D. E. Ellis, M. van Faassen, L. Fan, T. H. Fischer, C. Fonseca Guerra, A. Ghysels, A. Giammona, S. J. A. van Gisbergen, A. W. Götz, J. A. Groeneveld, O. V. Gritsenko, M. Grüning, S. Gusarov, F. E. Harris, P. van den Hoek, C. R. Jacob, H. Jacobsen, L. Jensen, J. W. Kaminski, G. van Kessel, F. Kootstra, A. Kovalenko, M. V. Krykunov, E. van Lenthe, D. A. McCormack, A. Michalak, M. Mitoraj, J. Neugebauer, V. P. Nicu, L. Noodleman, V. P. Osinga, S. Patchkovskii, P. H. T. Philipsen, D. Post, C. C. Pye, W. Ravenek, J. I. Rodríguez, P. Ros, P. R. T. Schipper, G. Schreckenbach, J. S. Seldenthuis, M. Seth, J. G. Snijders, M. Solà, M. Swart, D. Swerhone, G. te Velde, P. Vernooijs, L. Versluis, L. Visscher, O. Visser, F. Wang, T. A. Wesolowski, E. M. van Wezenbeek, G. Wiesenekker, S. K. Wolff, T. K. Woo, and A. L. Yakovlev, Amsterdam Density Functional, SCM, Theoretical Chemistry, Vrije Universiteit, Amsterdam, The Netherlands, https://www.scm.com, accessed 17 March.
[74]C. Adamo and V. Barone, "Toward reliable density functional methods without adjustable parameters: The PBE0 model," J. Chem. Phys. **110**, 6158–6170 (1999).
[75]J. Autschbach, "Magnitude of finite-nucleus-size effects in relativistic density functional computations of indirect NMR nuclear spin–spin coupling constants," ChemPhysChem **10**, 2274–2283 (2009).
[76]A. Klamt, "Conductor-like screening model for real solvents: A new approach to the quantitative calculation of solvation phenomena," J. Phys. Chem. **99**, 2224–2235 (1995).
[77]K. G. Dyall, "Relativistic double-zeta, triple-zeta, and quadruple-zeta basis sets for the 5*d* elements Hf–Hg," Theor. Chem. Acc. **112**, 403–409 (2004).
[78]K. G. Dyall, "Core correlating basis functions for elements 31–118," Theor. Chem. Acc. **131**, 1217 (2012).
[79]L. Jeremias, J. Novotny, M. Repisky, S. Komorovsky, and R. Marek, "Interplay of through-bond hyperfine and substituent effects on the NMR chemical shifts in Ru(III) complexes," Inorg. Chem. **57**, 8748–8759 (2018).
[80]W. Kutzelnigg, U. Fleischer, M. Schindler, and P. Diehl, "The IGLO-method: Ab initio calculation and interpretation of NMR chemical shifts and magnetic susceptibilities," in *Deuterium and Shift Calculation*, edited by E. Fluck, H. Gunther, R. Kosfeld, and J. Seelig (Springer-Verlag, Heidelberg, Germany, 1991), Vol. 23, pp. 165–262.
[81]M. Repisky, S. Komorovsky, M. Kadek, L. Konecny, U. Ekström, E. Malkin, M. Kaupp, K. Ruud, O. L. Malkina, and V. G. Malkin, "ReSpect: Relativistic spectroscopy DFT program package," J. Chem. Phys. **152**, 184101 (2020).
[82]P. A. M. Dirac, "Quantum mechanics of many-electron systems," Proc. R. Soc. London, Ser. A **123**, 714–733 (1929).
[83]A. D. Buckingham, T. Schaefer, and W. G. Schneider, "Solvent effects in nuclear magnetic resonance spectra," J. Chem. Phys. **32**, 1227–1233 (1960).
[84]M. Brehm and B. Kirchner, "TRAVIS—A free analyzer and visualizer for Monte Carlo and molecular dynamics trajectories," J. Chem. Inf. Model. **51**, 2007–2023 (2011).
[85]M. Brehm, M. Thomas, S. Gehrke, and B. Kirchner, "TRAVIS—A free analyzer for trajectories from molecular simulation," J. Chem. Phys. **152**, 164105 (2020).
[86]J. J. Wilson and S. J. Lippard, "Acetate-bridged platinum(III) complexes derived from cisplatin," Inorg. Chem. **51**, 9852–9864 (2012).
[87]J. Schagen, A. Overbeek, and H. Schenk, "Bis(μ-trifluoroacetato-O,O′)-bis[dimethyl(4-methylpyridine)platinum](Pt-Pt)," Inorg. Chem. **17**, 1938–1940 (1978).
[88]D. P. Bancroft, F. A. Cotton, L. R. Falvello, and W. Schwotzer, "Tetramethyldiplatinum(III) (Pt-Pt) complexes with 2-hydroxypyridinato bridging ligands," Inorg. Chem. **25**, 763–770 (1986).
[89]A. Marchenko, L. A. Truflandier, and J. Autschbach, "Uranyl carbonate complexes in aqueous solution and their ligand NMR chemical shifts and ^{17}O quadrupolar relaxation studied by ab initio molecular dynamics," Inorg. Chem. **56**, 7384–7396 (2017).
[90]N. Saeki, N. Nakamura, T. Ishibashi, M. Arime, H. Sekiya, K. Ishihara, and K. Matsumoto, "Mechanism of ketone and alcohol formations from alkenes and alkynes on the head-to-head 2-pyridonato-bridged cis-diammineplatinum(III) dinuclear complex," J. Am. Chem. Soc. **125**, 3605–3616 (2003).
[91]K. Matsumoto, S. Arai, M. Ochiai, W. Chen, A. Nakata, H. Nakai, and S. Kinoshita, "Synthesis of the pivalamidate-bridged pentanuclear platinum(II,III) linear complexes with Pt· · ·Pt interactions," Inorg. Chem. **44**, 8552–8560 (2005).
[92]N. Marino, C. H. Fazen, J. D. Blakemore, C. D. Incarvito, N. Hazari, and R. P. Doyle, "Isostructural Pd(II) and Pt(II) pyrophosphato complexes: Polymorphism and unusual bond character in d^8–d^8 systems," Inorg. Chem. **50**, 2507–2520 (2011).